

David C. Wendell and Robert M. Judd

Abstract

Cine cardiac imaging is the primary technique by which cardiovascular magnetic resonance (CMR) imaging characterizes regional and global contractile function of the heart and resulting blood flow through the great vessels. As such, cine imaging is of fundamental importance to clinical and research applications of CMR. The underlying technical challenge is to acquire high-quality images fast enough to characterize cardiac motion. A number of strategies have been developed to overcome this intrinsic challenge for MR-based imaging compared to real-time x-ray or ultrasound-based imaging. In general these strategies are highly successful, but typically involve trade-offs that vary somewhat depending on the health of the patient and the specific clinical question. In this chapter we review the fundamental principles of cine imaging, discuss the trade-offs associated with different strategies, and summarize these in the context of a typical CMR clinical service.

Keywords

Cine imaging • Contractile function • Cardiac magnetic resonance • Segmented k-space • Gradient echo imaging • Steady state free precession • Magnetic resonance imaging

Introduction

In general, magnetic resonance imaging can be divided into spin echo and gradient echo approaches. Compared to gradient echo imaging, spin echo imaging requires the use of a second, relatively time-consuming radiofrequency (RF)

pulse. Due to the need to image as fast as possible to characterize cardiac contraction, spin echo imaging is rarely used for cine cardiac imaging. Accordingly, spin echo imaging will not be described in this chapter.

Gradient echo imaging can be broadly divided into two categories, namely spoiled and refocused. In spoiled gradient echo imaging, the CMR signal derived from each radiofrequency excitation is independent of the CMR signal associated with previous RF excitations. From a technical perspective, a number of different strategies can be used to spoil or “erase” this historical dependence of the CMR signal. In refocused gradient echo imaging, conversely, an active attempt is made to preserve the CMR signal from RF pulse to RF pulse. This refocused state is relatively difficult for the CMR scanner hardware to achieve, but yields a significant increase in signal-to-noise ratio resulting in improved image quality. Both spoiled and refocused gradient echo imaging play an important role in CMR, and both are described in detail here following a brief introduction to the basic principles common to both.

Electronic supplementary material The online version of this chapter (doi:[10.1007/978-3-319-22141-0_10](https://doi.org/10.1007/978-3-319-22141-0_10)) contains supplementary material, which is available to authorized users.

D.C. Wendell, PhD
Department of Medicine/Cardiology, Duke Cardiovascular
Magnetic Resonance Center, Duke University Medical Center,
Durham, NC, USA
e-mail: david.wendell@duke.edu

R.M. Judd, PhD (✉)
Department of Medicine, Duke Cardiovascular Magnetic
Resonance Center, Duke University Medical Center,
Durham, NC, USA
e-mail: Robert.judd@duke.edu

Gradient Echo Imaging

Gradient echo imaging is a method of creating an MR image by imposing a magnetic field gradient across the desired imaging volume, and measuring resultant frequencies to encode frequency components from a given region. The pulse sequence is designed such that the readout gradient dephases the transverse magnetization, and then re-phases the magnetization to create an echo. The components of the gradient echo pulse sequence are outlined in Fig. 10.1, including RF pulse, slice, phase, and read encoding gradients.

What Is the FID?

Once the externally-applied RF signal has ended, H^1 spins will realign such that the net magnetic moment (M) is parallel to B_0 . During relaxation these H^1 spins lose energy by emitting their own RF signal, which is referred to as the free-induction decay (FID) response signal. These FIDs are measured by the receive coils placed around the body. The strength of the FID is dependent on the proton density of the tissue being imaged, the longitudinal relaxation time (T_1), and the transverse relaxation time (T_2). In theory, T_2 can be measured directly as the mono-exponential decay rate of the signal in a perfectly homogeneous magnetic field. By purposely applying magnetic field gradients, for example by

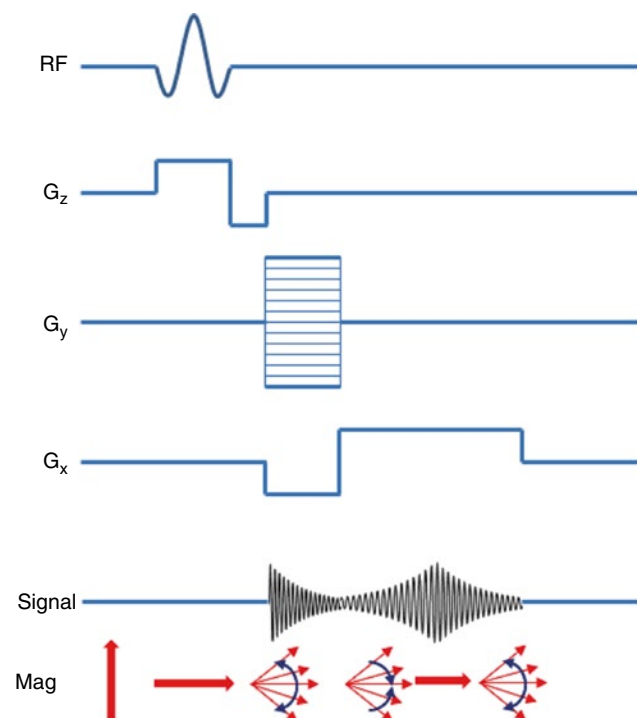


Fig. 10.1 GRE pulse sequence with resulting magnetization displayed at the *bottom*

slightly increasing the magnetic field experienced by the left side of the patient's body compared to the right side, the signal is forced to decay more quickly. Subsequent reversal of the gradient direction from left-right to right-left causes the formation of echoes (Fig. 10.1: Signal). The frequency components of these echoes contain information about spatial location, i.e. information regarding how much signal originated from the left versus right side of the patient's body, and therefore can be used to build an image.

What Are Echoes?

Unlike in a traditional spin-echo pulse sequence that uses 180° refocusing pulses, a gradient echo pulse sequence requires a bipolar readout gradient. This is achieved by first applying a dephasing gradient followed by the frequency-encoding readout gradient. The dephasing stage is inverse in sign and half the area of the frequency encoding gradient (see Fig. 10.1: G_x). This is designed such that the first half of the frequency-encoding gradient inverts the dephasing created by the negative lobe, and the peak of the echo occurs at the middle of the readout gradient (i.e. echo time (TE), Fig. 10.1: Signal).

Spoiled Gradient Echo Imaging (SPGR, FGRE, etc.)

The T_1 and T_2 times in the tissues involved in cardiac imaging are generally in the range of tens to hundreds of milliseconds. This means there is significant signal remaining in the transverse plane for repetition times normally used in cardiac imaging. In order to allow for fast cardiac imaging using GRE pulse sequences, the remaining magnetization should be 'spoiled' so it does not contaminate subsequent phase encoding steps. This can be accomplished either with gradient spoiling, which allows for shorter overall TR, or RF spoiling, which can facilitate T_1 weighting throughout the image acquisition.

Gradient Spoiling (Shortens TR)

Gradient spoiling is commonly used in cardiac imaging to destroy the residual transverse magnetization following each readout (Fig. 10.2). This is necessary to prevent transverse magnetization from previous RF pulses from contaminating subsequent readouts (known as stimulated echoes). The downside of gradient spoiling is the dephased spins no longer contribute to subsequent MR signals. Since the T_1 and T_2 of myocardium and blood are long, and TR is short, low flip angles are necessary to prevent loss of signal due to gradient spoiling [1].

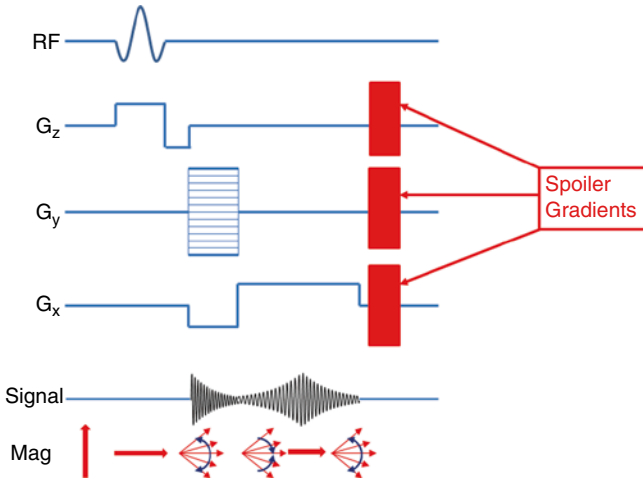


Fig. 10.2 Spoiled GRE pulse sequence showing spoiler gradients added at the end of each RF pulse

RF Spoiling

RF spoiling can also be referred to as RF pulse phase cycling. This takes advantage of the fact that the RF pulse can be played at any phase (i.e. direction in the x-y plane) and the refocusing occurs at that phase location. Therefore, if the RF pulse is played at a random phase, the likelihood that a stimulated echo will rephase at the same location is greatly reduced. In most practical applications the RF pulses played in a series of TRs are pseudo-random, incrementing phase quadratically to provide better spatially and temporally invariant spoiling than either gradient spoiling or completely random RF spoiling [2].

Signal Equation

The signal for a spoiled-GRE sequence depends on sequence-selectable variables (TR, TE, and flip angle (α)), along with three variables intrinsic to the tissue being imaged (T_1 , T_2^* , and spin density [H]). We have introduced a new term, T_2^* , rather than T_2 since the spoiled-GRE sequence does not account for field inhomogeneities as a spin-echo sequence would. Assuming we have reached a steady-state (see below) and have achieved perfect spoiling, the signal (S) of a spoiled-GRE sequence is given in Eq. 10.1

$$S = k[H] \frac{\sin \alpha (1 - e^{-TR/T_1})}{(1 - (\cos \alpha) e^{-TR/T_1})} e^{-TE/T_2^*} \quad (10.1)$$

where k is a scaling factor. The first term ($k[H]$) accounts for spin-density effects, the second term contributes to the T_1 weighting of the image, and the third term contributes to T_2^* weighting. From this, it is clear to see how α , TR, and TE contribute to T_1 and T_2^* weighting in spoiled-GRE sequences.

As α decreases, the T_1 effect is reduced ($1 - e^{-TR/T_1}$ term cancels), and we are left with [H] and T_2^* . If TR is long and TE is minimized, we are left with a proton-density weighted image. As the TE is increased, the amount of T_2^* weighting is increased. Conversely, as TR is decreased the amount of T_1 weighting actually increases (e^{-TR/T_1} term becomes large). Finally, if the TE is kept short (minimize T_2^*) and TR is short as well, α can be used to increase T_1 weighting as is given below [3].

To obtain the maximum signal, the optimal flip angle, called the Ernst angle (α_E), can be calculated by setting $dS/d\alpha = 0$ above.

$$\alpha_E = \arccos(e^{-TR/T_1}) \quad (10.2)$$

Saturation and In-Flow Effects

Using the explanation of spoiled-GRE signal and optimal flip angle above, it is easy to see how an aggressively high flip angle would tend to saturate the resulting spoiled-GRE signal. This saturation is more noticeable with shorter repetition times as are used for cardiac imaging. Basically, the acquisition is not allowing enough T_1 recovery between high flip angle RF pulses, so the majority of the MR signal is being spoiled, thus no longer contributing to subsequent MR signals.

The preceding derivation assumes everything within the imaging space has reached a steady-state. A more detailed description of steady-state imaging is provided below. For the discussion on inflow effects let's assume we are operating in a steady-state regime, which means the M_z signal returns to a consistent level between RF pulses. Now, assume there is inflowing blood from another part of the body, which has not been exposed to these RF pulses, and thus enters the imaging plane with a higher starting M_z than in-slice tissue. This results in a portion of the imaging plane not being in steady-state which manifests itself as signal inhomogeneities throughout the image (see blood pool in Fig. 10.3). The severity of this artifact is related to the tissue characteristics and imaging parameters chosen. The more saturated the steady-state signal (increased α , decreased TR), the larger the difference in M_z between steady-state and inflowing tissue, the more heterogeneous the signal appears [4].

Time to Steady State and the Role of Dummy Heartbeats

Performing spoiled GRE imaging requires the transverse and longitudinal magnetization to have achieved a steady state. This limits the fluctuation in magnetization from one RF

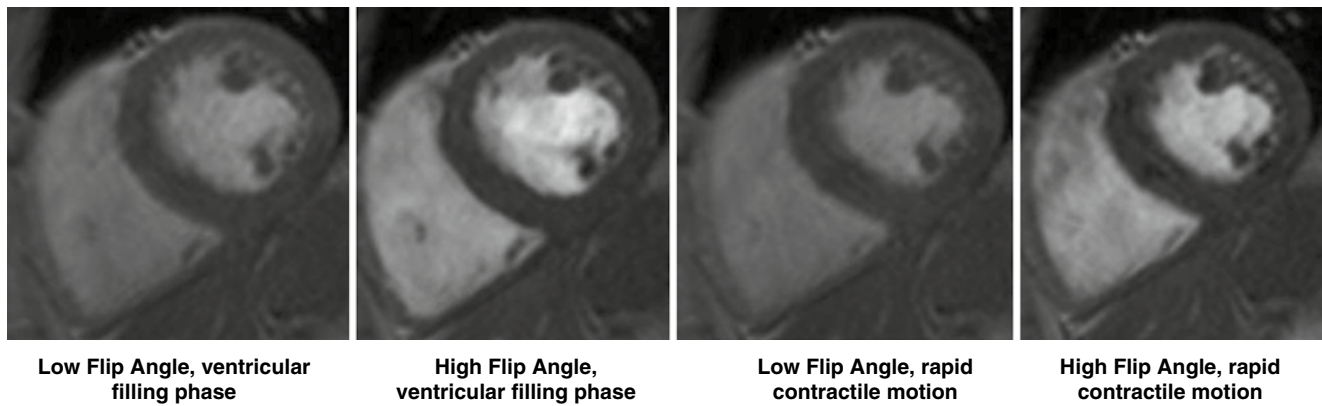


Fig. 10.3 Effects of high flip angle on spoiled GRE cine imaging. Note the heterogeneous blood signal during ventricular filling phase (*left*) due to inflowing spins. *Right*: myocardial heterogeneity due to rapid cardiac motion during relaxation

pulse to the next. The time it takes to reach a steady state depends on the MR parameters chosen (TR and flip angle) and inherent tissue properties such as T_1 .

To determine how many dummy RF pulses are required to reach steady-state, an experiment of repeated measures (RF pulses) can be performed empirically for a given set of tissue parameters. For example, the number of RF pulses required to reach 95 % of steady-state spoiled GRE signal for myocardium ($T_1 = 1,000$ ms, $T_2 = 45$ ms), with a TR/TE/flip angle of 10/2/15°, is 87 RF pulses (87×10 ms = 870 ms). For a patient with normal sinus rhythm (60–70 bpm), this would be one heartbeat worth of dummy pulses [5].

Dummy heartbeats can be included at the start of an acquisition to drive the spoiled GRE signal to steady-state prior to data acquisition. This is realized in the example described above. In this case a single heartbeat of dummy RF pulses would be sufficient to reach 95 % of the steady state signal. The number of dummy heartbeats can be adjusted as well due to differences in tissue T_1 , flip angle, TR, and patient heart rate. The accepted steady state tolerance may be decreased (from 95 % above, to 85 %), to prevent increasing overall scan time.

SNR Considerations for Rapid Imaging

Some compromises become necessary to perform rapid clinical cardiac MRI, for example, sacrifices in SNR in order to acquire the necessary data in a timely manner. Most of the acceleration techniques have a similar goal: to decrease the number of phase-encoding lines (and hence, RF pulses) required to reliably reconstruct an image. Non-symmetric fields of view or matrix dimensions can reduce the number of phase encoding steps required with no inherent loss in SNR. However, acquiring only a portion of k-space, either through partial Fourier acquisition, or acceleration techniques

such as GRAPPA or mSENSE, inherently alters the noise signature throughout the image and reduces SNR. Both of these techniques undersample the phase-encoding data during acquisition, and estimate the missing data during reconstruction. The resulting post-processed lines are created using these acquired lines. Therefore, the fewer true k-space lines acquired, the lower the overall SNR (reduced signal and increased noise).

Effect of Chemical Shift and Off-Resonance Effects

The Larmor frequency of a given H^1 spin can be calculated empirically from the gyromagnetic ratio (γ) and the B_0 field strength. However, H^1 spins behave differently depending on their chemical environment. For example, the Larmor frequency commonly associated with H^1 spins is calculated from water molecules. Chains of fatty acids have a different chemical environment, and hence a slightly different gyromagnetic ratio. This causes H^1 spins in fat to resonate at a slightly different frequency from water (220 Hz at 1.5 T, 440 Hz at 3.0 T).

This can be imagined as two wheels spinning at slightly different rates. The signal received by the scanner is combined of spins in fat and in water, but the scanner expects to receive a signal at the water H^1 Larmor frequency. Recall, frequency encoding gradient is used to record the excited spins from the imaged volume. If the H^1 spins in fat are precessing at a slightly different frequency, they will be localized to a slightly different position, or “shifted” along the frequency-encoding direction (Fig. 10.4).

Obviously the mis-localization of fat can be problematic if it obscures anatomy, or worse, is confused with pathology (i.e. fat within the myocardium). Therefore, adjustments in receiver bandwidth can reduce the amount of chemical shift

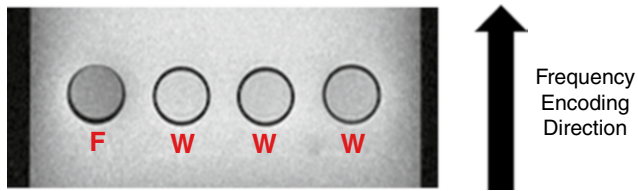


Fig. 10.4 MRI phantom showing chemical shift artifact (*F* fat, *W* water). With the frequency encoding direction from bottom to top, the fat tube (*F*) appears to be shifted 1–2 pixels higher than the water tubes. In reality, all tubes are in line

that occurs in an image. As an example, assume 1.5 T and a fat/water difference of 220 Hz. If our readout bandwidth is 220 Hz/pixel, then the fat will shift a full pixel in the frequency encoded direction, potentially confounding image interpretation. If the bandwidth were increased to 440 Hz, this shift would only be 0.5 pixels and the effect on image interpretation can be reduced [6].

Along the same lines as chemical shift artifacts, off-resonance effects can cause similar artifacts. In fact, chemical shift artifacts can be considered one specific type of off-resonance effect. In general, anything which causes a spin to precess at a resonant frequency which is different from its Larmor frequency can cause an off-resonance artifact. Off-resonance effects occur wherever a magnetic field gradient is present within the body. This could either be from intrinsic properties in the body (i.e. the “magnetizability” of tissue), or extrinsic sources such as eddy currents (produced from switching gradient coils on/off) or concomitant gradients (magnetic field changes orthogonal to applied magnetic field gradients). Overall, these effects result in a loss of signal in certain areas of the image due to a majority of H^1 spins no longer precessing at the expected frequency. These can manifest themselves as spatial distortion (images appear warped), signal loss (at interfaces between tissue and lung), blurring, or overall signal heterogeneity (similar tissue appears bright or dark throughout the image) [7].

Parameter Selection (BW, FA/Ernst Angle, TE, TR, Scan Time, etc.)

When setting up a clinical cine CMR study, certain trade-offs come into play when optimizing spatial and temporal resolution, SNR, scan time, breath-hold capability, and overall image quality. As described below, the top requirement of cine MRI would be to capture the fastest phases of cardiac motion during contraction and relaxation of the ventricle. This requires high temporal resolution on the order of about 20 cine frames per cardiac cycle. If the temporal resolution is too low the tradeoff is missing peak systole causing an overall underestimation of ejection fraction, blurring of

myocardium during cardiac motion, and inability to visualize wall motion abnormalities.

The required temporal resolution can be calculated by taking the patient’s average R-R interval, divide by 20 cine frames, and this produces the required temporal resolution. For example, a heart rate of 75 bpm is ~850 ms interval, if 20 cine frames are required, then the temporal resolution should be at least 42.5 ms. More details on setting optimal temporal resolution are included below.

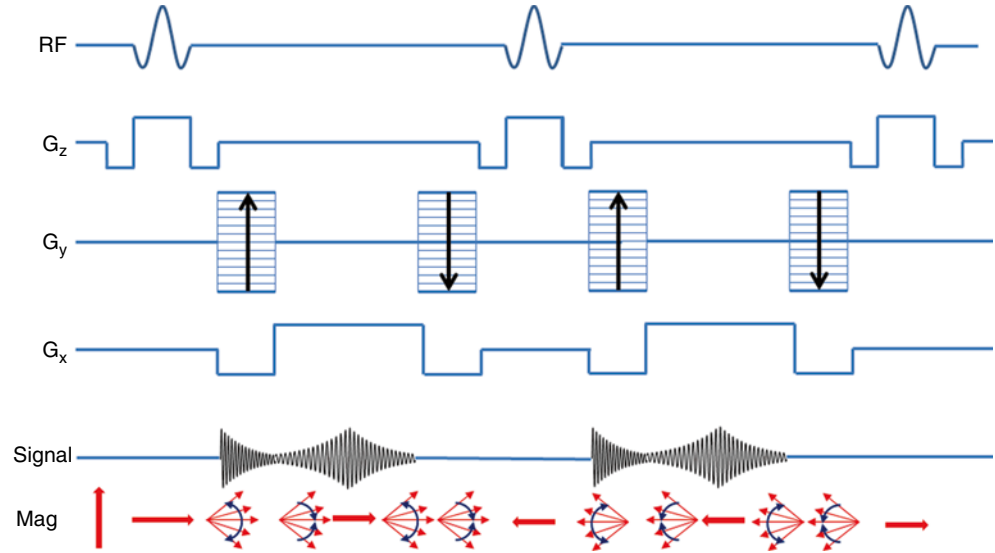
Another way to optimize signal in a spoiled GRE image are to calculate the Ernst angle, which was described in Eq. 10.2 above. TE and TR need to be minimized in order to allow for increased imaging speed and reduction in breath-hold duration. Increasing the bandwidth can reduce the chemical shift artifact. The trade-off of increasing the bandwidth is a decrease in SNR. Finally, spatial resolution needs to be of a level where one can reliably delineate the border between the blood pool and myocardium, and the myocardial wall itself. Sacrificing spatial resolution for reduced scan time may limit the number of imaging voxels present across the myocardium, which may cause blurring of the myocardium during the most vigorous cardiac motion.

Balanced Steady-State Free Precession (bSSFP)

One method to overcome the limitations of spoiled GRE imaging is, instead of destroying transverse magnetization after each RF pulse, the magnetization can be “recycled” to increase SNR and image contrast between blood and myocardium. The approach, referred to as balanced steady state free precession (bSSFP) imaging, can be thought of as a hybrid of a GRE image and a spin-echo image. The RF pulses are played at a flip angle which oscillates from pulse to pulse, the spacing between RF pulses is double the echo time, and imaging gradients are perfectly matched between RF pulses. This results in magnetization that perfectly refocuses at each TE and eliminates the loss of signal seen in spoiled GRE imaging (Fig. 10.5) [8].

bSSFP imaging has become the predominant cine imaging technique in most patients due to its high SNR, fast imaging speed, reduced flow dependency, and excellent blood to myocardium contrast. There are some caveats to these advantages. High flow velocity, metallic structures, and B_0 inhomogeneities can cause severe artifacts in bSSFP imaging. Because the magnetization is refocused there is a “history” present with the H^1 spins. Specifically, since spins are continually being refocused, if a spin is out of phase with other spins, the refocusing occurs at an arbitrary orientation, leading to signal loss. This is why artifacts from high velocity blood or metal implants are propagated through the image (see Video 10.1).

Fig. 10.5 bSSFP pulse sequence showing RF pulses, balanced gradients for slice encoding (G_z), phase encoding (G_y), and frequency encoding (G_x). Relative signal during each readout event (Signal), and resulting magnetization from each pulse sequence component (Mag)



Signal Equation

The signal for a bSSFP sequence depends on sequence-selectable variables (TR, TE, and flip angle (α)), along with three variables intrinsic to the tissue being imaged (T_1 , T_2 , and M_0). The steady-state equation for bSSFP signal is given in Eq. 10.3 below.

$$M_{ss} = M_0 \frac{\sqrt{\sin \alpha (e^{-TR/T_2}) (1 - e^{-TR/T_1})}}{1 - (e^{-TR/T_1} - e^{-TR/T_2}) \cos \alpha - (e^{-TR/T_1} e^{-TR/T_2})} \quad (10.3)$$

For short TR ($TR \ll T_1$ or T_2), which is the case for cardiac imaging, the exponentials in Eq. 10.3 can be approximated to $1 - TR/T_1$ and $1 - TR/T_2$, respectively. So Eq. 10.3 reduces down to:

$$M_{ss} = M_0 \frac{\sin \alpha}{\left(\frac{T_1}{T_2} + 1\right) - \cos \alpha \cdot \left(\frac{T_1}{T_2} - 1\right)} \quad (10.4)$$

It can be seen from Eq. 10.4, that the signal generated from a bSSFP image relies solely on flip angle (α) [8]. Therefore, to optimize signal from tissues, the Ernst angle (α_E) can be calculated as follows:

$$\alpha_E = \arccos \left(\frac{T_1 - T_2}{T_1 + T_2} \right) \quad (10.5)$$

SNR is increased by the re-wound gradients seen in Fig. 10.5 and in tissues with a T_2/T_1 ratio close to 1 (i.e. blood has a T_2/T_1 of 0.15 v. myocardium which is 0.0375).

Saturation and Inflow Effects

Fortunately, since the “recycling” feature of bSSFP imaging retains some of the magnetization, a high flip angle does not

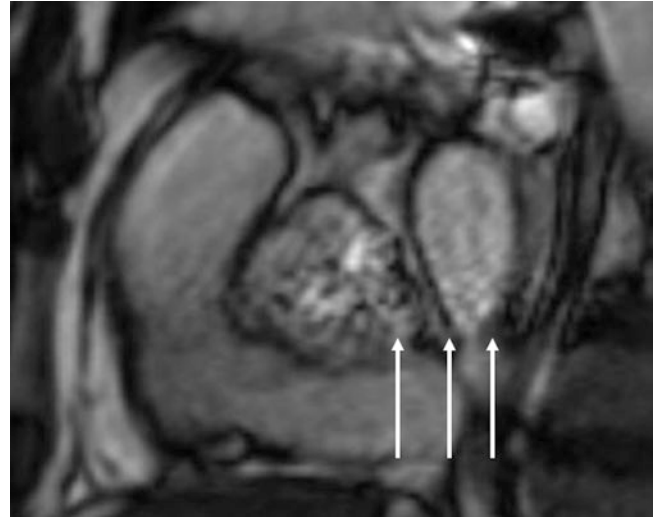


Fig. 10.6 Ringing in the frequency-encoding direction (arrows) due to high, fully relaxed blood signal entering the imaging plane in bSSFP imaging

have the saturation effect seen in spoiled GRE imaging. However, the likelihood of reaching specific absorption rate (SAR) limits, i.e. exposing the patient to excessive RF radiation, prohibits excessively high flip angles.

One common artifact seen in bSSFP imaging pertains to inflowing blood. Because by definition the MRI signal needs to be at steady-state, any spins entering the imaging plane which are not at steady state result in a larger starting M_0 than spins within the imaging slice. This discrepancy can cause ringing artifacts throughout the image in the phase-encoding direction (see Fig. 10.6). The main difference in inflow effects in bSSFP imaging compared to spoiled GRE imaging is the inherent “history” in the SSFP signal. Since magnetization is continually refocused, the discrepancy between incoming and steady state spins persists until the incoming spins reach steady state. The severity of this

artifact is related to the tissue characteristics and imaging parameters chosen. The higher the velocity of incoming blood the more discrepant the starting magnetization, and the more dramatic the artifact. Imaging parameters such as higher flip angles, or longer TR (and inherently TE since $TR=2 \times TE$ for bSSFP imaging), can exacerbate these artifacts as well [9].

Prep Pulses and Time to Steady State, Dummy Heartbeats

Similar to the discussion in the spoiled GRE section, bSSFP imaging requires the magnetization to have reached at steady state. The fluctuations in magnetization from one RF pulse to the next can have detrimental effects on image quality, especially since traveling spins tend to have a “memory” from previous RF pulses. As described above, the first RF pulse played is actually $\alpha/2$ followed by a series of α pulses which oscillate from $+x$ to $-x$ to establish a steady-state. The number of the pulses required to reach steady state depend on TR, flip angle, and tissue properties (T_1).

The method to determine the number of RF pulses required to reach steady state can be determined implicitly. For example, if we assume a threshold of 95 % of steady-state signal, the signal from myocardium ($T_1=1,000$ ms, $T_2=45$ ms), and a TR/TE/flip angle of 3/1.5/50°, then the number of RF pulses required to reach steady state is 76. However, most scanners will ramp up the beginning RF pulses to eliminate the high oscillations associated with these sequences. For example, 10 RF pulses at increasing flip angle may be used at the start of the sequence to more smoothly drive the signal to a steady state. Using this scheme, the number of leading RF pulses can be reduced to 46, well within a single dummy heartbeat [10].

SNR Efficiency/Fast Imaging

The bSSFP sequence itself is inherently faster than spoiled GRE imaging due to the shorter repetition time and higher bandwidth. High bandwidth imaging tends to reduce overall SNR, but the higher flip angle implemented within bSSFP imaging compensates for some of this loss. Similar acceleration techniques are still employed within cine cardiac imaging using bSSFP sequences to reduce imaging time and create reasonable breath hold durations. The overall goal in reducing imaging time is undersampling of k-space lines in the phase encoding direction. Accelerated imaging can be obtained by intuitively prescribing imaging planes, for example, orienting the phase-encoding direction along the narrower dimension of the image (anterior/posterior direction). This allows non-symmetric fields of view or matrix dimensions to reduce the number of phase encoding lines without the risk of image wrap obscuring anatomy. Other

techniques such as acquiring only a portion of k-space, either through partial Fourier acquisition, or acceleration techniques such as GRAPPA or mSENSE, inherently alters the noise signature throughout the image and reduces SNR. These techniques selectively undersample k-space data using an algorithm which allows the back-calculation of the missing k-space data to avoid image wrap. In brief, these techniques acquire a central core of k-space lines around $k_x = 0$ (24–36 lines), and then selectively undersample k-space lines moving outward towards higher k_y lines. The scheme can either sample every other line (referred to as GRAPPA 2), or the algorithm can sample only every third line (GRAPPA 3). Both techniques will reconstruct the imaging data by filling in the missing k-space lines using the data acquired from prior and subsequent k-space lines. However, the fewer acquired lines, and the more interpolated lines, the more the image will suffer from increased noise, decreased SNR, and imaging artifacts. Therefore, the fewer true k-space lines acquired, the lower the overall SNR (reduced signal and increased noise).

Effects of Chemical Shift and Off Resonance

Chemical shift artifacts and off resonance effects become more noticeable due to the tight timing constraints on bSSFP imaging, and the “memory” encoded into spins as they are imaged repeatedly using the bSSFP sequence. Chemical shift effects were discussed in the spoiled GRE section, but a different type of chemical shift is present in bSSFP imaging. Pass bands were described previously in relation to the appearance of stop-bands within bSSFP images. It turns out that, because of the bandwidth used in bSSFP imaging, the signal peaks from water and fat (440 Hz/pixel at 3 T) occur in opposite frequency lobes. This results in signal loss at the interfaces between fat and water. This “india ink” artifact is due to the presence of fat and water within the same voxel in the image. If we assume a 50/50 fat/water voxel in a bSSFP image, where fat and water are out of phase with each other, the sum of the vectors within this voxel adds up to zero (Fig. 10.7).

Off resonance effects have a large impact on bSSFP cine imaging. The timing between RF pulses in the “balanced” SSFP is set such that spins are refocused at each echo time. The off-resonance effects within the image cause changes in the magnetic field, which cause spins to precess at a different rates, thus inhibiting the refocusing that is essential to bSSFP imaging. These effects can be seen as dark bands throughout the image either near tissue interfaces, near metallic implants, or regions of high flow. Figure 10.8 shows dephasing artifacts in bSSFP imaging due to high flow through aortic regurgitant orifice (top) and aortic stenosis (bottom). Dephasing of spins near metallic implants propagate throughout the image in bSSFP imaging (Fig. 10.9), but are contained to the region surrounding the metallic implant in spoiled GRE imaging (Fig. 10.9, Video 10.1 and 10.2).

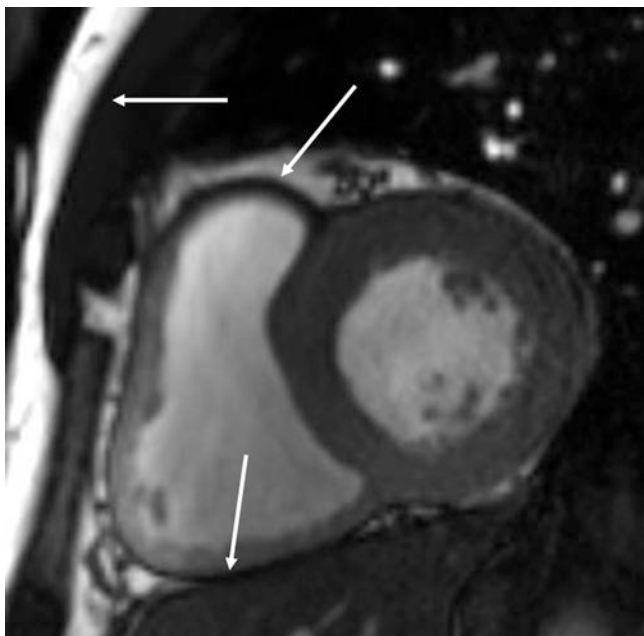


Fig. 10.7 bSSFP cine imaging showing chemical shift artifact (arrows) due to water and fat occupying the same voxel causing signal cancellation

The presence and location of artifacts from off-resonance effects can be reduced by creating a more homogeneous magnetic field through magnet shimming, decreasing the repetition time (which increases the spacing between stop bands), or applying a frequency shift which moves the stop bands out of the imaging area of interest [10].

Parameter Selection (BW, FA/Ernst Angle, TR, TE, Frequency Scout)

Overall, the goal of parameter selection for bSSFP imaging is rapid imaging, good myocardial/blood contrast, adequate spatial and temporal resolution, and high SNR. The high temporal resolution is achieved by reducing the TR (and TE, which is $1/2 \times TR$ for bSSFP) by increasing the bandwidth. The decrease in SNR due to the higher bandwidth in bSSFP imaging is counteracted by the high flip angles available due to spin “recycling.” The flip angle does have an upper limit, which is related to SAR.

Temporal and spatial resolutions need to be optimized similar to spoiled GRE imaging. High temporal resolution is necessary to accurately capture rapid systolic motion of the heart. To visualize small structures, high spatial resolution is required as well. The benefit of bSSFP over spoiled GRE is the short TR allows for better spatial and temporal resolution without extending imaging time and breath hold duration.

The overall benefits of bSSFP over spoiled GRE are high SNR, good conspicuity of myocardium and blood, and shorter breath hold imaging. However, susceptibility artifacts pose a larger challenge due to the “memory” inherent to

bSSFP imaging. Therefore, for most cine imaging studies, bSSFP is the desired imaging sequence, but in situations where metal artifacts, B_0 inhomogeneity, or inflow artifacts obscure the structures of interest, spoiled GRE imaging can be used. The drawbacks of lower myocardial/blood contrast and longer scan times may offset some of the difficulties associated with imaging artifacts. These effects may be more prominent at 3 T. The trade-offs with specific consideration to cardiac imaging will be discussed in the next section.

Cardiac Imaging

For both spoiled and refocused gradient echo imaging approaches, modern CMR scanner hardware can typically achieve a repetition time (TR) between RF excitations of roughly 3–8 ms. The number of excitations (k-space lines) needed to obtain reasonable image spatial resolution of the human heart is roughly 120–180. Even with a TR of 3 ms and only 120 k-space lines, total imaging time is 360 ms, yielding approximately three images per second. This temporal resolution is too slow to examine cardiac contraction.

The most widely used approach to address this limitation is segmented k-space data acquisition, first described by Edelman et al. in the late 1980s [11]. The underlying concept is similar to that used for gated SPECT. Specifically, the image data are acquired over several consecutive cardiac cycles, and then combined during image reconstruction to produce a composite movie loop depicting a single cardiac cycle. In practice the CMR data are typically acquired while the patient holds their breath in order to eliminate respiratory motion, and total acquisition time for a single movie loop is typically 8–12 s. Breath hold image acquisitions typically result in movie loops comprised of 16–24 movie frames across the entire cardiac cycle (systole and diastole).

Segmented k-Space

The basic principles of segmented k-space imaging are shown in Fig. 10.10. Note that k-space represents the raw data for the image, such that filling the lines of k-space is synonymous with acquiring the resulting image (the gray-scale image is obtained by performing a two dimensional Fourier transform on the k-space data).

In PANEL A of Fig. 10.10, the patient has just started holding their breath, and the first cardiac cycle has begun. At this time k-space lines 1, 2, 3, and 4 of the first movie frame are acquired. Rather than continuing to acquire k-space lines 5, 6, 7, etc. of the first movie frame, however, the CMR scanner is programmed to acquire lines 1, 2, 3, and 4 of the second movie frame (PANEL B of Fig. 10.10). This process continues until lines 1, 2, 3, and 4 of all movie frames have been acquired, which is timed to complete at the end of the first cardiac cycle.

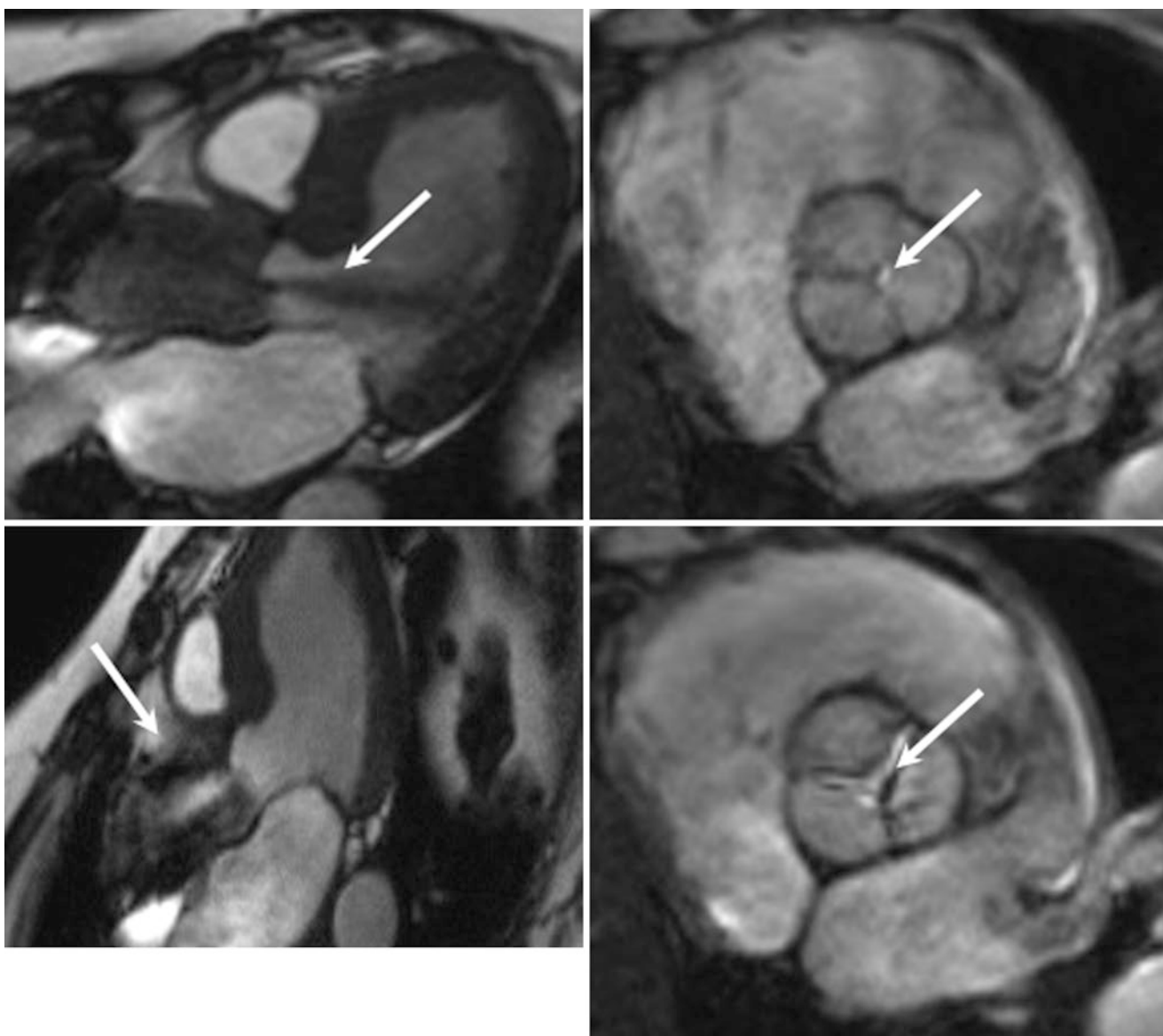


Fig. 10.8 bSSFP cine imaging showing dephasing of spins (*arrows*) due to high flow in a patient with aortic insufficiency (*top*) and a patient with aortic stenosis (*bottom*) (en face view of aortic valve shown at *right*)

At this point (end of first cardiac cycle) all movie frames have some k-space data (lines 1, 2, 3, and 4), but no movie frames have all k-space data (no lines 5 or greater).

In PANEL C of Fig. 10.10 the second cardiac cycle begins, and lines 5, 6, 7, and 8 of the first movie frame are acquired (lines 5–8 are white, lines 1–4 are red). In PANEL D of Fig. 10.10, lines 5, 6, 7, and 8 of the second movie frame are acquired. At the end of the second cardiac cycle all movie frames have 8 k-space lines (lines 1–8).

This process continues during subsequent cardiac cycles until all movie frames have all k-space lines, at which point the grayscale movie loop depicting cardiac contraction can be reconstructed by applying a two dimensional Fourier transform to the raw k-space data.

The basic equations used by the CMR scanner to segment k-space are:

$$\text{Heart Beats} = \frac{\text{Total Lines}}{\text{Segments}}$$

$$\text{Number of Movie Frames} = \frac{\text{Acquisition Window}}{(\text{Segments} \cdot \text{Time Per Line})}$$

Perhaps the most important variable in these equations is “segments”, which represent the number of k-space lines acquired for each movie frame in a single cardiac cycle. In the example of Fig. 10.10, segments = 4.

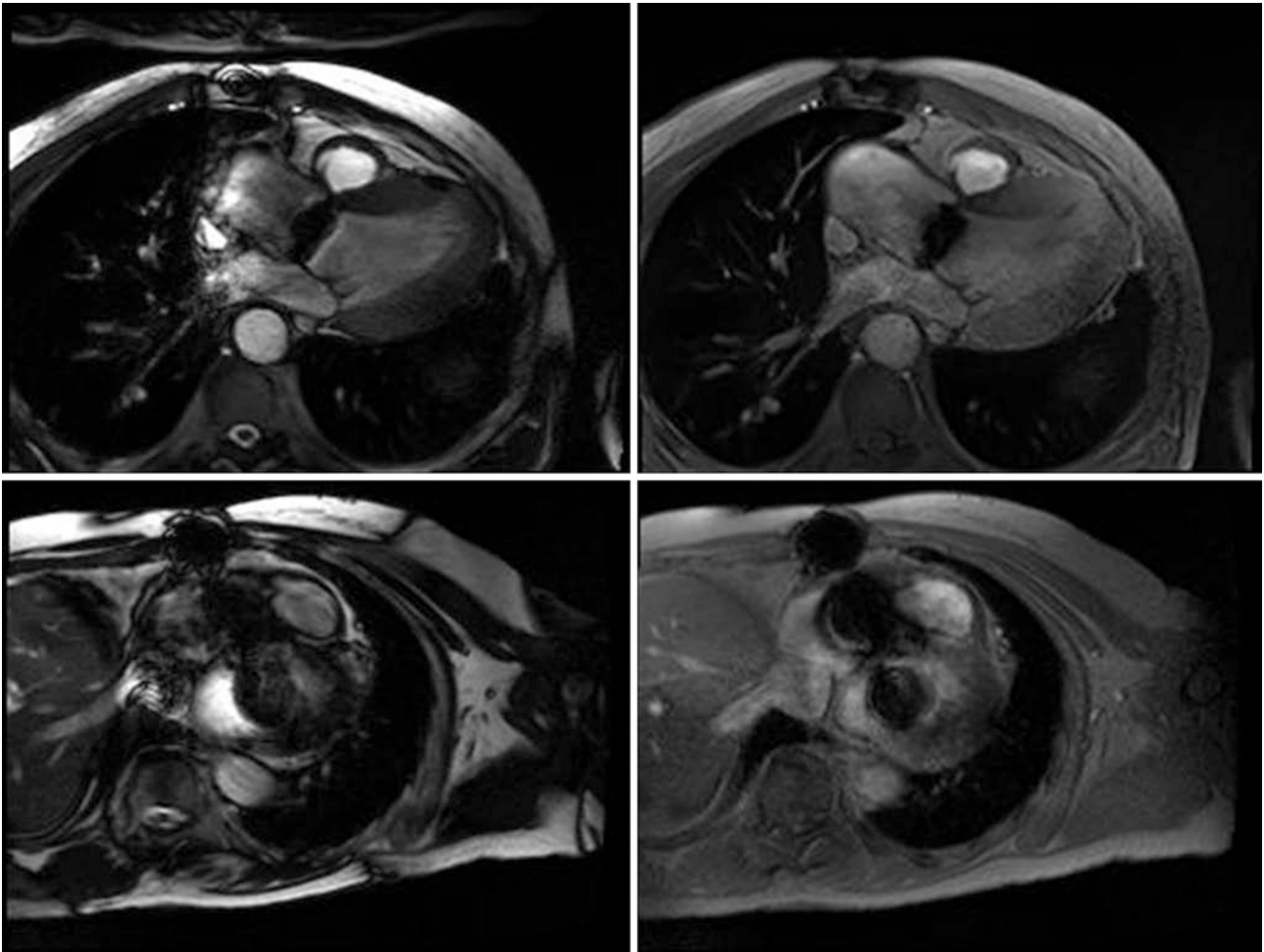


Fig. 10.9 bSSFP cine imaging showing dephasing of spins due to metallic implants (*top*: mechanical aortic valve, *bottom*: mechanical aortic and mitral valve). bSSFP show large artifacts obscuring most

heart structures, spoiled GRE (*right*) show localized artifacts with the majority of cardiac structures visible

Typical values for “total lines” and “segments” would be 192 and 14. Using the first equation with these values, breath hold duration would be 14 heart beats (192/14). Using the second equation, and assuming a typical value of 750 ms for the “acquisition window” (essentially the cardiac R-R interval) and a value of 3 ms for “time per line” (the TR for a bSSFP imaging pulse sequence), the number of movie frames would be 20 ($750/\{14 \text{ times } 3\}$). In a clinical setting the CMR scanner operator would adjust these values based on the patient’s heart rate and the patient’s ability to repeatedly hold their breath in order to obtain the best image quality with the most movie frames.

Breath-Holding

Clinical imaging generally involves choosing the best trade-offs for the current patient. If the patient is relatively healthy

and can hold their breath for 15–20 s, more movie frames and/or images with better spatial resolution (more “total lines”) can be acquired. It’s important to recognize, however, that each movie requires a separate breath hold, and that the patient will need to hold their breath many times during the overall 30–60 min CMR procedure. In clinical practice we have found that even relatively ill cardiac patients can repeatedly hold their breath for 10 s, corresponding to roughly 18 movie frames and 2 mm spatial resolution for a typical modern CMR scanner.

For those patients that cannot hold their breath, and/or have irregular heart rates due for example to atrial fibrillation, segmented k-space image acquisition cannot be used. In these patients the only practical approaches involve sacrificing image quality. Perhaps the most common approach for patients that cannot breath hold is sacrificing image signal-to-noise and spatial resolution to the point where poor-quality images are acquired every 100 ms (ten images per

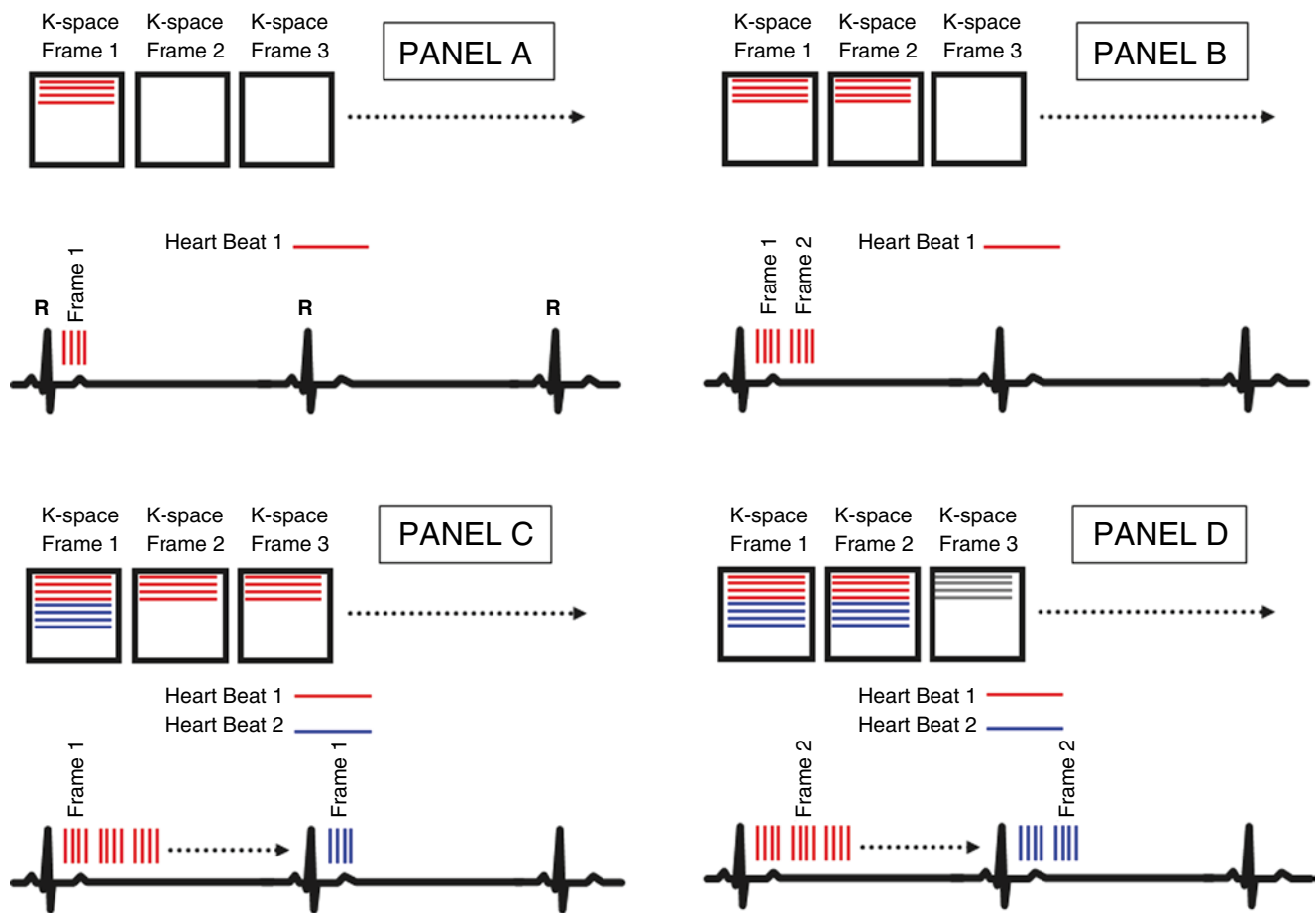


Fig. 10.10 Segmented k-space image acquisition. Within each cardiac cycle, some but not all data are acquired for each movie frame. No movie frames are complete until the last cardiac cycle, during which all

movie frames are completed. Panel A: First heart beat, first movie frame. Panel B: First heart beat, second movie frame. Panel C: Second heart beat, first movie frame. Panel D: Second heart beat, second movie frame

second), typically referred to as “real time” imaging. Other approaches have also been described, but regardless of the approach image quality is significantly reduced in patients that cannot repeatedly hold their breath, and/or have irregular heart rates.

Retrospective Gating

The preceding technique, where the MRI scanner hardware is triggered in synchrony with cardiac contraction, is referred to as prospective gating. Retrospective gating, conversely, involves acquiring not only the k-space lines but also the patient’s R wave (see Fig. 10.11). Relatively complex image reconstruction techniques are then applied after data acquisition (after the breath hold) to arrange the k-space lines across consecutive cardiac cycles in such a way that the resulting data are similar to prospective gating (Fig. 10.11). Until the early twenty-first century retrospective gating reconstruction algorithms were problematic, and most CMR imaging employed prospective gating. In recent years, however,

retrospect gating reconstruction algorithms have improved significantly, and the use of retrospective gating has become increasingly common in the clinical setting.

Retrospective gating has the advantage that the final 10–50 ms of the cardiac cycle is well characterized, whereas this time period is generally ignored with prospective gating due to the need for the CMR scanner to “listen” for the next R-wave. This difference is particularly important for velocity-encoded imaging, where the loss of flow data near the end of diastole can introduce significant errors (ca. 20 %) in estimates of arterial and venous flows.

View Sharing

View sharing essentially involves interpolating k-space data across movie frames in order to shorten breath hold times. As shown in Fig. 10.12, k-space lines in movie frame 1 and 3 are acquired by the scanner (solid lines), whereas the k-space lines for movie frame 2 are interpolated (dotted lines). View sharing typically involves the interpolation of some, but not

Fig. 10.11 Retrospective gating. Both the k-space data and the R-wave trigger are recorded. Specialized reconstruction software retrospectively distributes the k-space lines amongst the movie frames

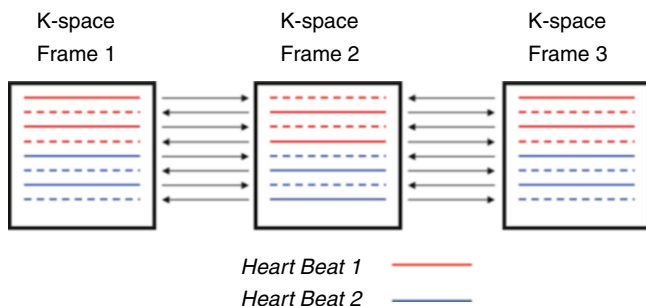
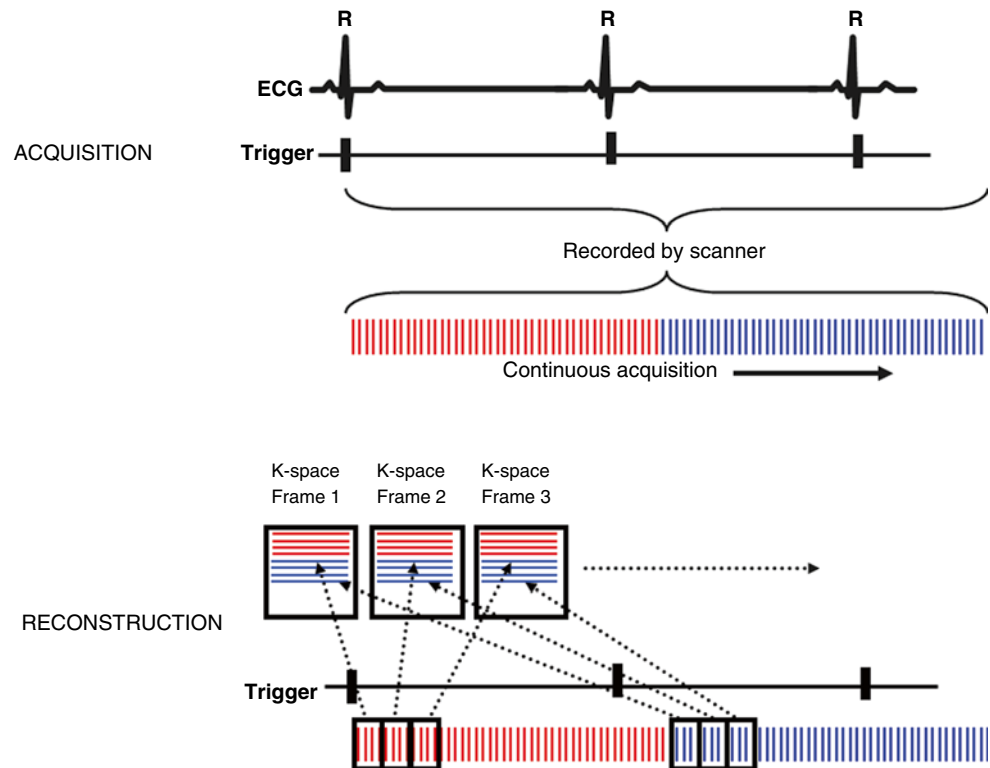


Fig. 10.12 View sharing. Solid k-space lines are acquired. To shorten overall movie acquisition time (breath hold time), dotted k-space lines are not actually acquired but rather are calculated as the average of the corresponding lines from the previous and next movie frames

all, k-space lines in order to minimize the negative effects of interpolation. The trade offs of view sharing are conceptually similar to those obtained by any other interpolation technique, namely some of the data is essentially fictitious. The use of view sharing in the clinical setting has in general become less common in recent years, perhaps in part because parallel imaging techniques offer similar reductions in breath hold duration with less loss of information.

Partial Fourier, Parallel Imaging

Parallel imaging techniques, such as GRAPPA and mSENSE, are based on a clever idea first described in the late 1990s

[12–14]. The underlying idea is that each of the multiple radiofrequency receiver coils placed around the patient's thoracic cavity contains differing spatial information, and that by incorporating this information during the image reconstruction process some k-space lines can be constructed without acquiring them directly.

Over the past decade a family of these techniques has developed and matured, each with characteristic advantages and disadvantages. For cardiovascular imaging, the primary advantage of all parallel imaging techniques is that they reduce patient breath hold durations. The primary disadvantage is a loss of signal-to-noise, but for a given reduction in breath hold duration the loss of signal is smaller than would occur with alternative approaches. Because of this, parallel imaging represents a major advance for cine cardiac imaging. The conceptual details of the various techniques themselves are complex, and beyond the scope of this chapter. From the perspective of the scanner operator, conversely, implementing these techniques is so simple that virtually all routine clinical CMR scans incorporate some form of parallel imaging.

Clinical Applications

When Is bSSFP Appropriate?

For both our inpatient and outpatient MRI scanners at Duke University Hospital, most patients have a steady heart rate and can repeatedly hold their breath for 10–12 s. In these

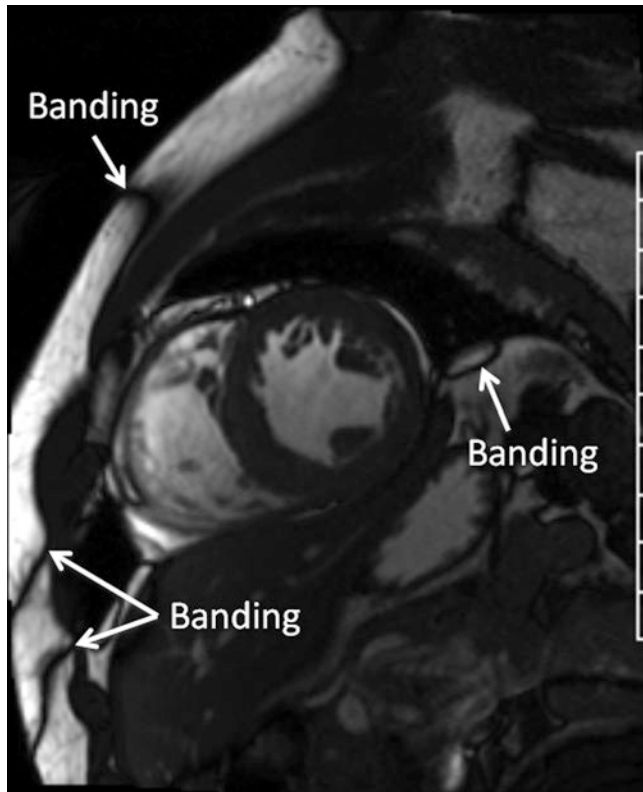


Fig. 10.13 bSSFP imaging at 3T. Overall image quality is excellent. Although banding artifacts are present, their position does not obscure the areas of diagnostic interest

patients, balanced SSFP cine imaging is arguably the clear choice and its use is often recommended in society guidelines [15, 16]. Image signal to noise is generally excellent, and the short TR allows more than adequate spatial and temporal resolution. The resulting movie loops are typically far more than adequate for careful inspection of regional and global wall motion, and often reveal subtle structures and blood flow patterns than are not available using any other CMR technique or other imaging modality.

At 1.5 T, artifacts for bSSFP are relatively infrequent. At 3 T artifacts are more frequent and, when present, typically appear in the chest wall and/or in the inferior portion of left ventricular free wall adjacent to the lung. In these regions the air/water interface causes local inhomogeneities in the static magnetic field, resulting in local destruction of the MRI signal and, therefore, dark bands. Perhaps the best way to address this issue is by applying 3D shimming techniques locally around the heart, rather than across the entire body, in order to improve homogeneity in the region of diagnostic interest (the heart). If shimming is not successful, the dark bands can be moved (but not eliminated) away from the heart and large vessels by small manual changes in transmitter frequency (eg. 50 Hz). Fig. 10.13 and Video 10.3 show 3 T bSSFP images with artifactual dark bands located away from the heart, i.e. away from the areas of diagnostic importance

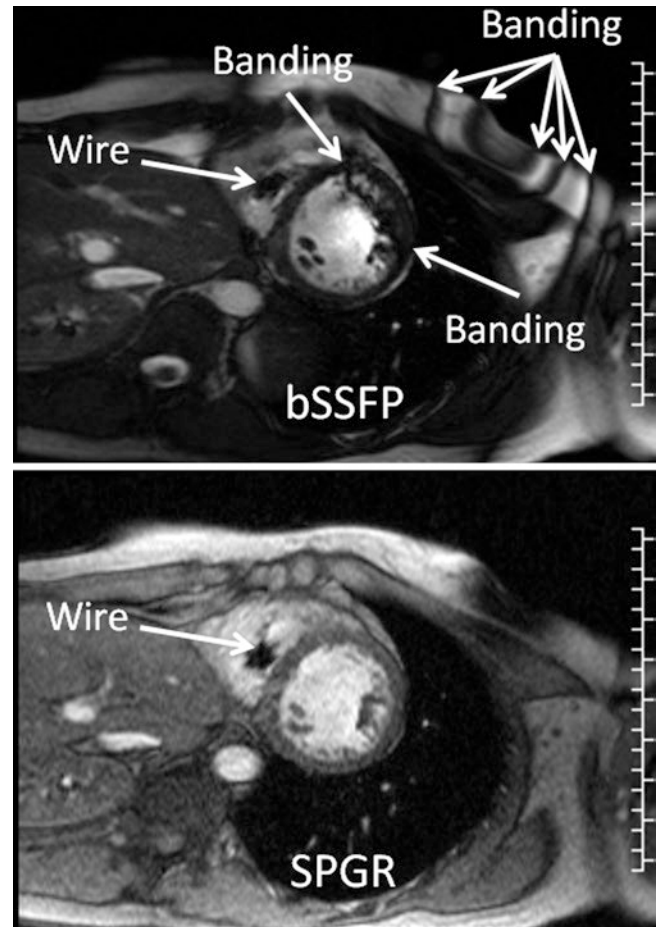


Fig. 10.14 Cine imaging in a patient with a pacemaker. bSSFP imaging exhibit severe artifacts (*top*) that can be avoided by using SPGR imaging instead (*bottom*)

to CMR. Note that the heart itself has excellent image quality, and even subtle structures like trabeculae can be visualized in detail. Occasionally, even the chordae connecting papillary muscles to the leaflets of the mitral and aortic valves can be visualized.

When Is SPGR Cine Appropriate?

In some patients, especially those with metallic implants or severe iron overload, the dark bands on bSSFP images cannot be successfully moved away from the heart, even by a combination of shimming and transmitter frequency shifting. In these patients the best strategy is to use spoiled GRE (SPGR) techniques instead. Figure 10.14 and Video 10.4 show an example of a patient with a pacemaker in whom bSSFP images resulted in a dark band through the LV free wall, precluding confident interpretation of wall motion in this area. The SPGR images (Video 10.5), conversely, are free of this artifact because SPGR imaging is much less dependent on magnetic field homogeneity. Because mag-

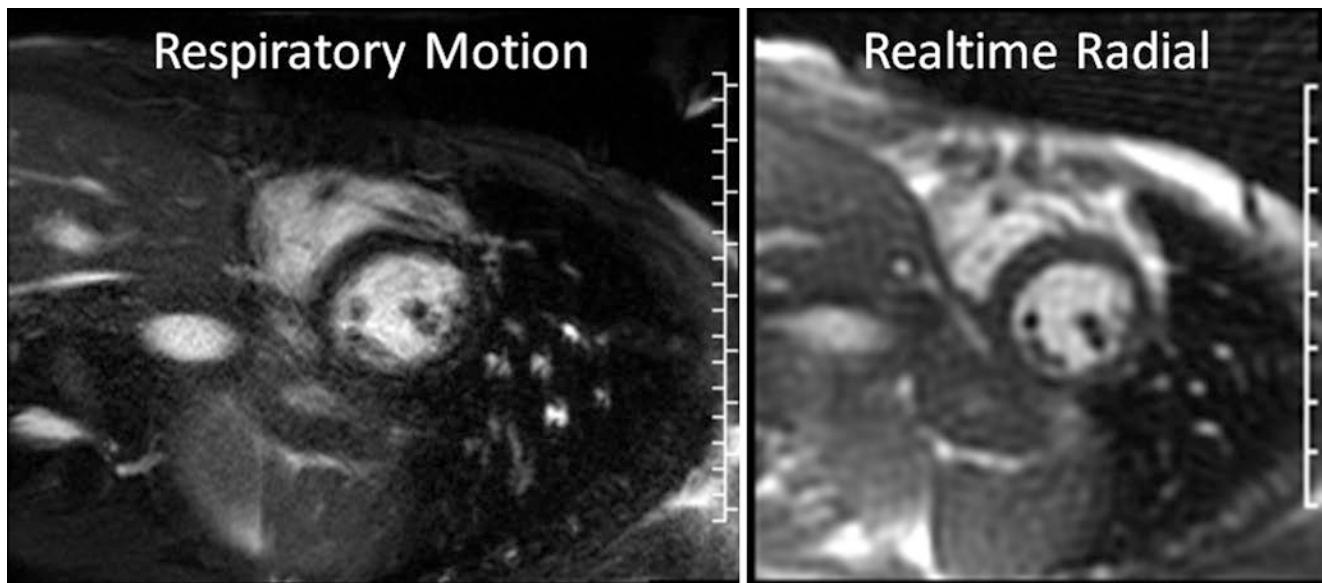


Fig. 10.15 ECG gated (*left*) and real-time (*right*) imaging in a patient that could not hold their breath

netic field inhomogeneities increase with field strength, the need to use SPGR instead of bSSFP is more common at 3 T compared to 1.5 T. An additional advantage of SPGR is that patient exposure to RF radiation is lower, typically reported by the scanner as specific absorption rate (SAR), due to the use of a lower imaging flip angle and a longer TR. In some circumstances the need to lower SAR alone may motivate the use of SPGR as opposed to bSSFP.

When Is Real-Time Cine Appropriate?

In patients with arrhythmia and/or an inability to hold their breath, ECG gating is typically not clinically practical. Cine imaging is still possible in these patients, but all current approaches result in poorer image quality. Real-time cine imaging may actually be preferred in some instances where beat-to-beat variation in wall motion helps make the diagnosis, such as the respiratory variation of septal motion in pericardial disease with constrictive physiology. Arguably the best choice in this circumstance is to use real-time cine imaging, which as previously described involves trading off spatial resolution and image quality to achieve image acquisition times of approximately 100 ms. At ten images per second the real-time CMR images begin to resemble images from echocardiography, i.e. the images are acquired and displayed during cardiac contraction. Figure 10.15 and Videos 10.6 (bSSFP) and 10.7 (SPGR) show an example of a patient that could not hold their breath. The gated images are of poor quality and arguably not clinically useful. The real-time images,

conversely, are at least clinically useful even though they are significantly worse than gated bSSFP or SPGR. Note that the real-time images portray several cardiac cycles, as with echocardiography, as opposed to one cycle played in a loop for bSSFP and SPGR. As described above, this is because the bSSFP and SPGR movie frames are reconstructed to represent a composite cardiac cycle (segmented k-space gating).

References

1. Wood ML, Silver M, Runge VM. Optimization of spoiler gradients in FLASH MRI. *Magn Reson Med.* 1987;5(6):455–63.
2. Crawley AP, Wood ML, Henkelman M. Elimination of transverse coherences in FLASH MRI. *Magn Reson Med.* 1988;8(3):248–60.
3. Buxton RB, Edelman RR, Rosen BR, et al. Contrast in rapid MR imaging: T1- and T2-weighted imaging. *J Comput Assist Tomogr.* 1987;11(1):7–16.
4. Han M, Hargreaves BA. Reduction of flow artifacts by using partial saturation in RF-spoiled gradient-echo imaging. *Magn Reson Med.* 2011;65(5):1326–34.
5. Busse RF, Riederer SJ. Steady-state preparation for spoiled gradient echo imaging. *Magn Reson Med.* 2001;45:653–61.
6. Smith RC, Lange RC, McCarthy SM. Chemical shift artifact: dependence on shape and orientation of the lipid-water interface. *Radiology.* 1991;181(1):225–9.
7. Ferreira PF, Gatehouse PD, Mohiaddin RH, et al. Cardiovascular magnetic resonance artefacts. *JCMR.* 2013;15:41–80.
8. Nayak KS, Lee HL, Hargreaves BA, et al. Wideband SSFP: alternating repetition time balanced steady state free precession with increased band spacing. *Magn Reson Med.* 2007;58(5):931–8.
9. Amano Y, Nozaki A, Takahama K, et al. Reduction in flow artifacts by using interleaved data acquisition in segmented balanced steady

- state free precession cardiac MRI. *Comput Med Imaging Graph*. 2005;29(6):441–5.
10. Scheffler K, Lehnhardt S. Principles and applications of balanced SSFP techniques. *Eur Radiol*. 2003;13:2409–18.
 11. Atkinson DJ, Edelman RR. Cineangiography of the heart in a single breath hold with a segmented turbo-FLASH sequence. *Radiology*. 1991;178:357–60.
 12. Sodickson DK, Manning WJ. Simultaneous acquisition of spatial harmonics (SMASH): fast imaging with radiofrequency coil arrays. *Magn Reson Med*. 1997;38:591–603.
 13. Pruessmann KP, Weiger M, Scheidegger MB, et al. SENSE: sensitivity encoding for fast MRI. *Magn Reson Med*. 1999;42:952–62.
 14. Griswold MA, Jakob PM, Heidemann RM, et al. Generalized auto-calibrating partially parallel acquisitions (GRAPPA). *Magn Reson Med*. 2002;47:1202–10.
 15. Kramer CM, Barkhausen J, Flamm SD, Kim RJ, Nage E. Society for cardiovascular magnetic resonance and board of trustees task force on standardized protocols: standardized cardiovascular magnetic resonance (CMR) protocols 2013 update. *J Cardiovasc Magn Reson*. 2013;15:91.
 16. Hundley WG, Bluemke DA, Finn JP, et al. ACCF/ACR/AHA/NASCI/SCMR 2010 Expert consensus document on cardiovascular magnetic resonance, a report of the American College of Cardiology Foundation Task Force on Expert Consensus Documents. *J Am Coll Cardiol*. 2010;55(23):2619.